Supplementary Section

Topographical biomaterials instruct bacterial surface attachment and the *in vivo* host-pathogen response

Manuel Romero[1], Jeni Luckett[1], Grazziela Figueredo[2], Alessandro M. Carabelli[3], Aurélie Carlier[4], Aliaksei Vasilevich[5], Steven Vermeulen[4,5], David Scurr[3], Andrew L. Hook[3], Jean-Frédéric Dubern[1], David Winkler[6], Amir Ghaemmaghami[7], Jan de Boer[5], Morgan R Alexander[3†] and Paul Williams[1†*]

[1]National Biofilms Innovation Centre, Biodiscovery Institute and School of Life Sciences, University of Nottingham, Nottingham, United Kingdom.
[2]School of Computer Science, University of Nottingham, Nottingham United Kingdom
[3]Advanced Materials and Healthcare Technologies Division, School of Pharmacy, University of Nottingham, Nottingham, United Kingdom.
[4]Laboratory for Cell Biology-Inspired Tissue Engineering, MERLN Institute for Technology-Inspired Regenerative Medicine, Maastricht University, Maastricht, the Netherlands.
[5]BioInterface Science lab, Department of Biomedical Engineering, Eindhoven University of Technology, Eindhoven, the Netherlands.
[6]Department of Biochemistry and Genetics, La Trobe Institute for Molecular Science, La Trobe University, Kingsbury Drive, Melbourne, Victoria 3086, Australia and Monash Institute of Pharmaceutical Sciences, Monash University, Parkville, Australia
CSIRO Data61, Pullenvale, Australia,
[7]School of Life Sciences, University of Nottingham, Nottingham, United Kingdom.

1. Data Analysis

Cell Profiler analysis of topography images provided 66 uncorrelated topographical shape descriptors that were used to train *P. aeruginosa* and *S. aureus* attachment models. The full set of topographical descriptors is listed in **Table S2**. For *P. aeruginosa,* 1,852 TUs were investigated and for *S aureus* 2,084 were considered. TUs were excluded from the analysis if their signal to noise ratio was lower than 2.

The XGBoost machine learning method and Multiple Linear Regression with Expectation Maximisation (MLREM)(Burden and Winkler, 2009) were both used to generate non-linear and linear relationships between the topographies and bacterial attachment, producing good models for the datasets. Those methods were coupled with Shappley Additive Explanation (SHAP)(Lundberg and Lee, 2017) method for descriptor selection. The models were built based on the top ten most informative descriptors for each dataset, as identified by SHAP. All methods were implemented in Python 3.7. XGBoost version 0.22 using default parameters was employed to generate the ML models. Seventy percent of each dataset was used to train the models, and 30% were kept aside in a test set used to determine the predictive power of the models.

Although XGBoost has produced a better non-linear fit to the data (with R^2 = 0.82 and RMSE 0.27 log fluorescence for *P. aeruginosa;* and R^2 = 0.79 and RMSE 0.20 log fluorescence for *S. aureus* in the test set), MLREM regression coefficients assisted informing the individual contribution of each descriptor to attachment (**Figs 2B and 2F**). MLREM results showed that there is also a strong linear correlation between the selected descriptors and bacterial attachment, with R^2 = 0.71 and RMSE 0.34 log fluorescence for *P. aeruginosa;* and R^2 = 0.71 and RMSE 0.24 log fluorescence for *S. aureus* in the test set.

References

Burden, F.R.; Winkler D.A. Optimum QSAR Feature Selection using Sparse Bayesian Methods, QSAR Comb Sci. 2009; 28: 645-653

Lundberg SM, Li S-I. A unified approach to interpreting model predictions. In *Advances in Neural Information Processing Systems*, 2017. Pp 4765–4774.

Table S1: Bacterial strains, plasmids and primers used in this study

Strain, plasmid or primer	Genotype and/or Relevant characteristic	Source or reference
Strain		
P. aeruginosa		
PAO1-L	Wild type PAO1 strain, Lausanne subline	B. Holloway via D. Haas
PAO1-W	Wild-type PAO1 strain, Washington subline	Washington collection
PAJD431	In frame deletion of *pilA* in PAO1-W	This study
PAJD477	In frame deletion of *fliC* in PAO1-W	This study
S. aureus		
SH1000	Wild-type	Horsburgh et al., 2002
Pr. mirabilis		
Hauser 1885	Wild-type	Hauser, 1885
A. baumannii		
ATCC17978	Wild-type	Baumann et al., 1968
E. coli		
DH5α	*recA1 endA1 hsdR17 supE44 thi-1 gyrA96 relA1 ∆(lacZYA-argF)U169[ϕ80 dlacZ∆M15],* Nal^R	Liss, 1987
S17.1λpir	*thi pro hsdR hsdM*$^+$ *recA RP4-2-Tc::Mu-Km::Tn7 λpir*, Gm^R	Simon *et al.*, 1983
Plasmids		
pME3087	Suicide vector for homologous recombination, ColE1 replicon, Mob; Tc^R	Voisard *et al*., 1994
pJD112	pME3087 derivative for the generation of *pilA* in frame deletion mutant; Tc^R.	This study
pJD113	pME3087 derivative for the generation of *fliC* in frame deletion mutant; Tc^R.	This study
P*cdrA*::*gfp*^{S}	pUCP22Not-P*cdrA*-RBS-CDS-RNaseIII-*gfp*(Mut3)-T0-T1, Ap^R Gm^R; c-di-GMP reporter	Rybtke *et a*l 2012
Primers		
PilAΔ FW1	5'-ATATCTAGAATGCCGAACTGCTCG-3'	This study
PilAΔ RV1	5'-TTAGTTATCACAACCTTGAGCTTTCATGAATCTCTC-3'	This study
PilAΔ FW2	5'-TTCATGAAAGCTCAAGGTTGTGATAACTAAGGTGAT-3'	This study
PilAΔ RV2	5'-TATCTGCAGAAGTGGAAGTGGAGA-3'	This study
FliCΔ FW1	5'-ATATCTAGAATGCTCGAAGGCGCGCATCT-3'	This study
FliCΔ RV1	5'-TTAGCGCAGCAGGCTTGTAAGGGCCATGGTGATTTC-3'	This study
FliCΔ FW2	5'-ACCATGGCCCTTACAAGCCTGCTGCGCTAAGCCCGG-3'	This study
FliCΔ RV2	5'-TATAAGCTTAAGTCGTTCAACCCGCGCGT-3'	This study

References for Supplementary Table S1

1. Horsburgh MJ, Aish JL, White IJ, Shaw L, Lithgow JK, Foster SJ. sigmaB modulates virulence determinant expression and stress resistance: characterization of a functional rsbU strain derived from Staphylococcus aureus 8325-4. J Bacteriol 2002;184(19):5457–5467.
2. Hauser G. Über fäulnissbacterien und deren beziehungen zur septicämie. Ein betrag zur morphologie der spaltpilze. Leipzig, Germany: Vogel 1885.
3. Baumann P, Doudoroff M, Stanier RY. A study of the Moraxella group. II. Oxidative-negative species (genus Acinetobacter). J Bacteriol 1968;95(5):1520–1541.
4. Liss LR. New M13 host: DH5αF' competent cells. Bethesda Research Laboratories FOCUS 1987;9:3-5.
5. Simon R, Priefer U, Pühler A. A Broad Host Range Mobilization System for In Vivo Genetic Engineering: Transposon Mutagenesis in Gram Negative Bacteria. Nat Biotechnol 1983;1:784–791.
6. Voisard C, Bull C, Keel C, Laville J, Maurhofer M, Schnider U, Défago G, Haas, D. Biocontrol of root diseases by Pseudomonas fluorescens CHA0: Current concepts and experimental approaches. In: Molecular Ecology of Rhizosphere Microorganisms 1994;67-89. O'Gara F, Dowling D, Boesten B, eds. VCH Publishers, Weinheim, Germany.

Table S2: TopoUnit topographical surface descriptors

Surface property	**Description**
NumTri	The number of triangles used
NumLine	The number of lines used
CircDiam	Circle diameter
TriSize	Length of the shortest side of a triangle
LineLen	Line length
RotSD	The standard deviation (in degrees), is used to determine the rotation of the primitives when they are placed in the feature
CircArea	The area of circle primitives
TriArea	The area of triangle primitives
LineArea	The area of line primitives
Total Area	The total area occupied by primitives
DT	The number of triangle primitives scaled by feature area
DL	The number of line primitives scaled by feature area
CA	The total area of circle primitives scaled by feature area
TA	The total area of triangle primitives scaled by feature area
CCD	Number of colour changes of the feature over the diagonal
Pillars Number [2]	Number of micro-pillars per TopoUnit area
Pattern Area[2]	The actual number of pixels in the region per TopoUnit area
Compactness[2]	The variance of the radial distance of the object's pixels from the centroid divided by the area
Eccentricity[2]	The eccentricity of the ellipse that has the same second-moments as the region. The eccentricity is the ratio of the distance between the foci of the ellipse and its major axis length. The value is between 0 and 1. (0 and 1 are degenerate cases; an ellipse whose eccentricity is 0 is actually a circle, while an ellipse whose eccentricity is 1 is a line segment.)
Extent[2]	The proportion of the pixels in the bounding box that are also in the region. Computed as the Area divided by the area of the bounding box.
Form Factor[2]	Calculated as 4*π*Area/Perimeter2. Equals 1 for a perfectly circular object.
Major axis length[2]	The length (in pixels) of the major axis of the ellipse that has the same normalized second central moments as the region.

Surface property	Description
Min Feret Diameter[2]	The Feret diameter is the distance between two parallel lines tangent on either side of the object (imagine taking a caliper and measuring the object at various angles). The minimum Feret diameter is the smallest possible diameter, rotating the calipers along all possible angles.
Median Radius[2]	The median distance of any pixel in the object to the closest pixel outside of the object.
Max Radius[2]	The maximum distance of any pixel in the object to the closest pixel outside of the object. For skinny objects, this is 1/2 of the maximum width of the object.
Orientation[2]	The angle (in degrees ranging from -90 to 90 degrees) between the x-axis and the major axis of the ellipse that has the same second-moments as the region.
Perimeter[2]	The total number of pixels around the boundary of each region in the image.
Solidity[2]	The proportion of the pixels in the convex hull that are also in the object, i.e. ObjectArea/ConvexHullArea. Equals 1 for a solid object (i.e., one with no holes or has a concave boundary), or <1 for an object with holes or possessing a convex/irregular boundary.
Inscribed Circle[2]	The inscribed circles of a defined minimum diameter found between objects
Pillars Number	The total number of pillar primitives in the topo unit

Each micro-topographical element contains primitives (circles, triangles and rectangles). Features are repeated to cover the surface of a TopoUnit. For each of the descriptors derived from Image Analysis of bright field images, area and shape features are extracted, each parameter has an additional subset of descriptors including; standard deviation, mean, median, mad, minimum, maximum, variance, skewness, mode and percentile (0.1, 0.25, 0.5, 0.75 and 0.9) measurements.

TopoChip surface chemistry

As surface chemistry has a profound impact on bacterial attachment, it was essential to ensure that it was consistent across all the TUs. We therefore subjected the TopoChips to time-of-flight secondary ion mass spectrometry (ToF-SIMS) for molecular characterization with high lateral resolution together with X-ray photoelectron spectroscopy (XPS) for quantitative elemental analysis. Both methods detected F impurities on the array surface, with XPS providing quantification for each TU on the array, e.g. topography T2-PS-1228 [F] = 2.2 ± 0.3 at% (**Fig S2A**). This could be assigned to residues from a monolayer of trichloro(1*H*,1*H*,2*H*,2*H*-perfluorooctyl)silane (FOTS) deposited on the OrmoStamp mould to facilitate moulding (Zhao et al., 2017). The distribution of F on the TU features, side walls and valleys was found to be constant using ToF-SIMS, within the limits of the technique imposed by the artefactual distortion of the features observed in **Fig. S2B**. Presenting a range of TUs where the F to C ratio was quantified by XPS, **Fig. S2C** illustrates that there was no statistically significant difference between the units (one-way ANOVA, $p>0.05$). These results indicate that the surfaces used in the screening have uniform chemistry and that the bacteria-material interactions observed are specifically dependent on surface topography.

Since TSB containing 10% serum (TSBHS10%) was used to simulate *in vivo* growth for some experiments, XPS analysis was carried out after incubation of TUs in uninoculated TSBHS10% medium for 4 h. No significant differences in the protein layer thicknesses were recorded between different TUs (**Fig. S2C**). Higher levels of N were detected on topographically defined surfaces compared to flat controls after TSBHS10% conditioning, corresponding with an increase in protein layer thickness (**Fig. S2C**). However, it is likely that the differences originate from the reduced sampling depth on the vertical feature sides that results in an over-estimation of protein layer thickness.

SUPPLEMENTARY FIGURES

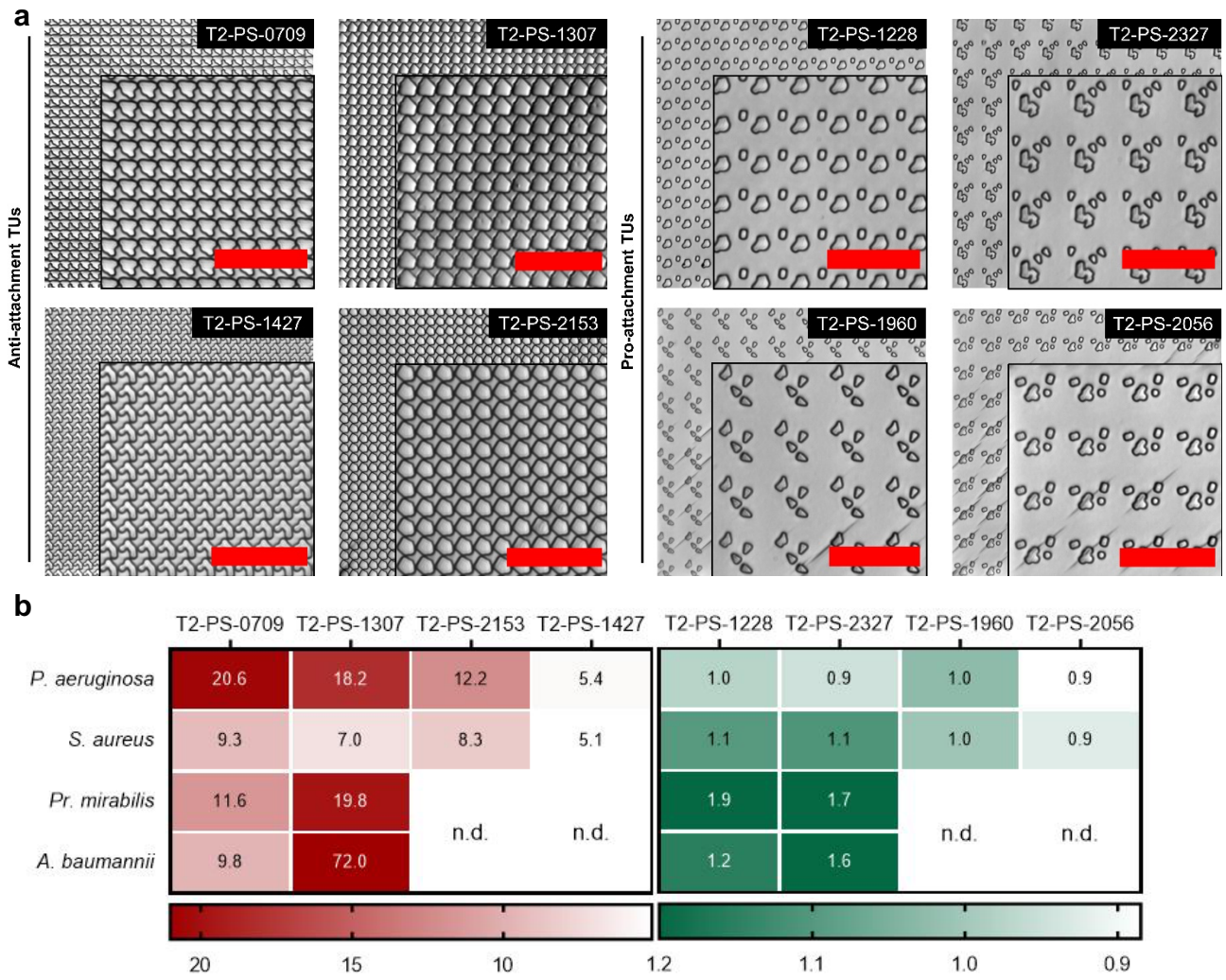

Figure S1. Selected anti- and pro-attachment micro-topographies (**a**) based on the screening data obtained from quantifying *P. aeruginosa* and *S. aureus* attachment to PS TopoChips. (**b**) Intensity maps of the fold reduction (red) or increase (green) in the measured fluorescence of the flat control for *P. aeruginosa*, *S. aureus*, *Pr. mirabilis* and *A. baumannii* attachment to the same PS TUs. Scale bar: 50 µm.

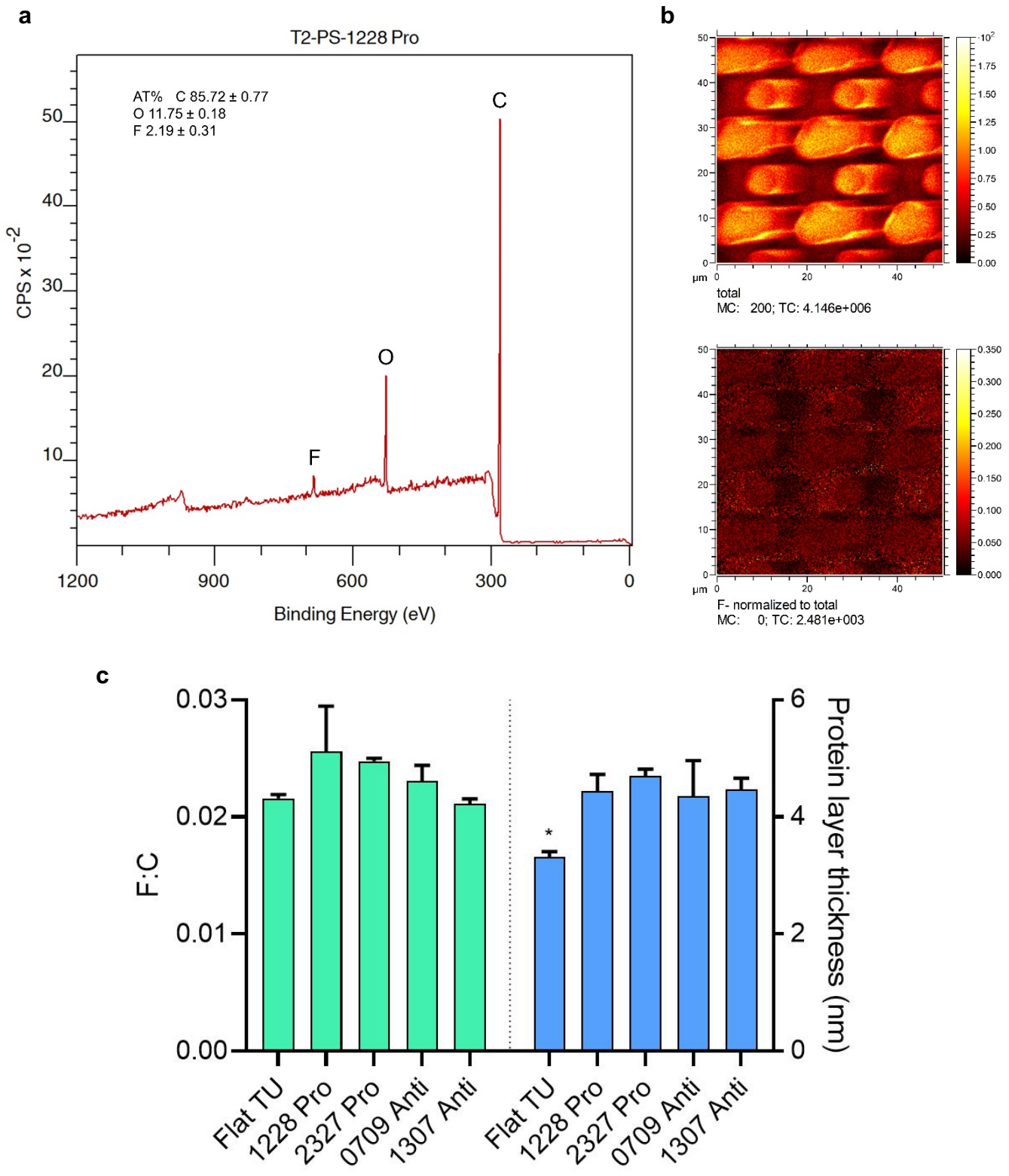

Figure S2. PS TopoChip surface chemistry analysis. (**a**) Representative XPS spectrum, obtained from a 100 × 100 µm area corresponding to a pro-attachment TU (T2-PS-1228) in a plasma-treated chip, showing F impurity originated from PS TopoChip demoulding procedure. Atomic % for C, O and F elements are shown. (**b**) ToF-SIMS total negative and normalized F polarity secondary ion images obtained from a 50 x 50 µm area corresponding to TU (T2-PS-1228) showing no differences in F content between topographical features of the same pattern. (**c**) Calculated F:C ratios from TUs with pro and anti-attachment properties against bacteria compared to flat surface control in PS TopoChip (green bars). Protein depth (nm) associated with pro and anti-attachment TUs and flat control after conditioning in TSBHS10% cell culture

medium for 4 h (blue bars). Statistical differences between group means were determined by one-way ANOVA tests (*p<0.05).

a

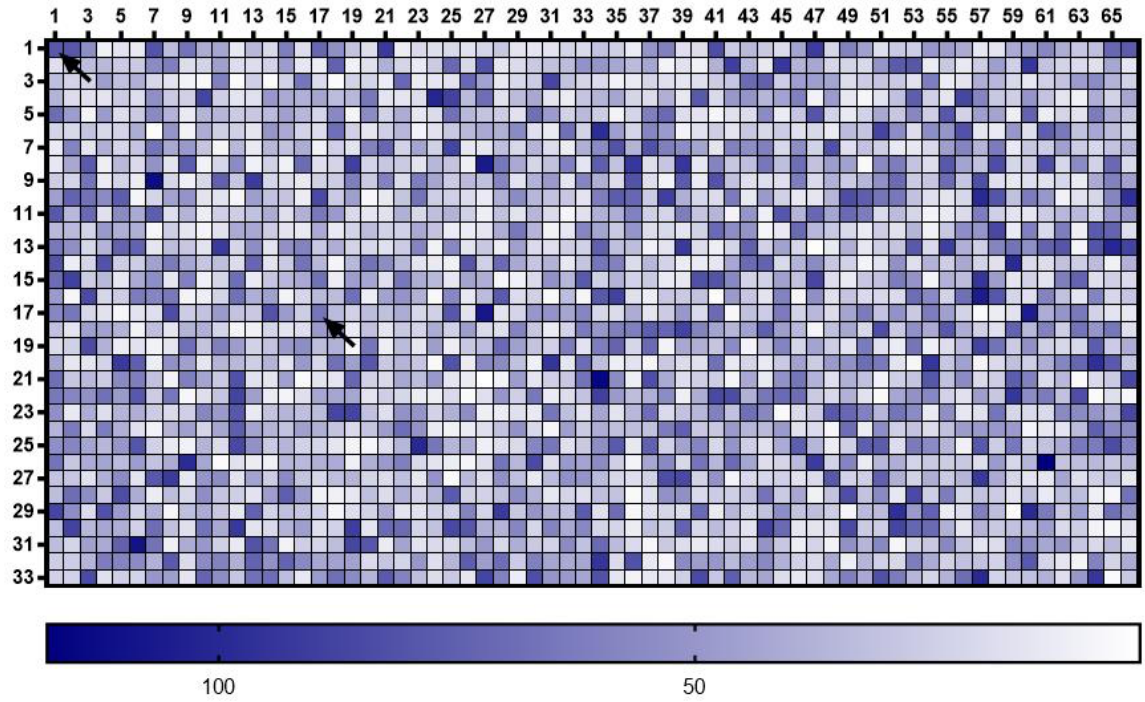
1 3 5 7 9 11 13 15 17 19 21 23 25 27 29 31 33 35 37 39 41 43 45 47 49 51 53 55 57 59 61 63 65
1 3 5 7 9 11 13 15 17 19 21 23 25 27 29 31 33
100
50

b

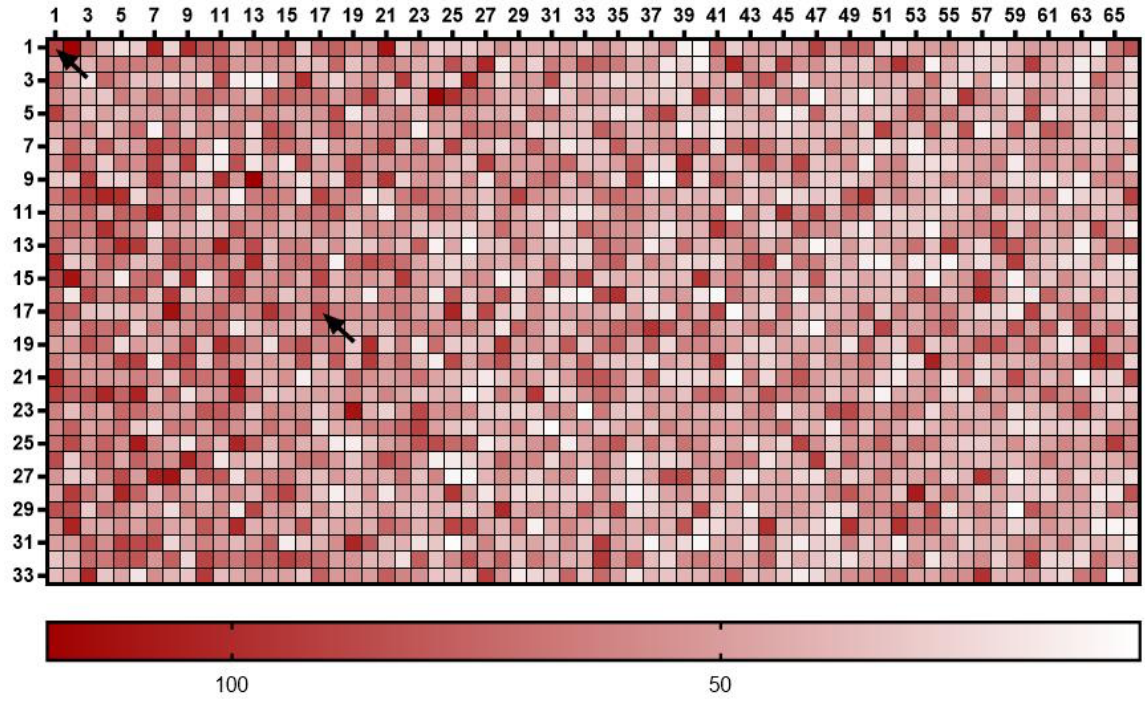
1 3 5 7 9 11 13 15 17 19 21 23 25 27 29 31 33 35 37 39 41 43 45 47 49 51 53 55 57 59 61 63 65
1 3 5 7 9 11 13 15 17 19 21 23 25 27 29 31 33
100
50

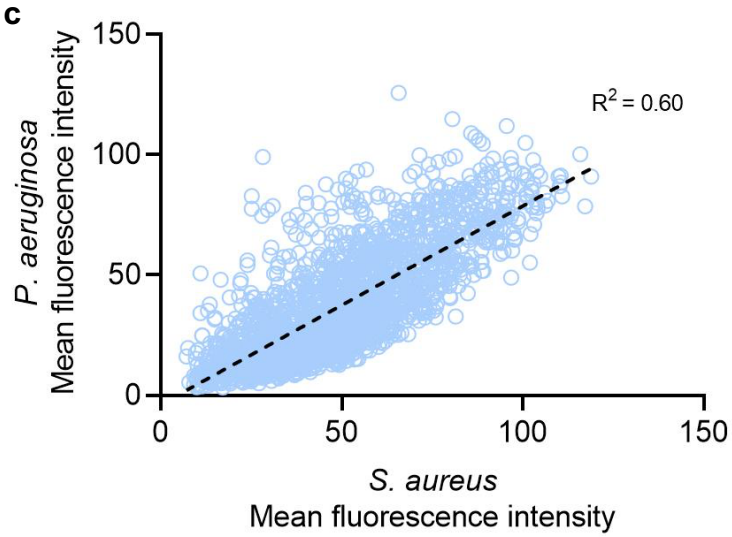

Figure S3. Intensity maps of measured fluorescence of *P. aeruginosa* (**a**) and *S. aureus* (**b**) attached to TUs from PS TopoChips after 4-h incubation. Shading within each outlined square indicates the mean fluorescence intensity value for the TU (Key to bottom). Black arrows pointing towards the TU coordinates 1,1 and 17,17 indicate flat surface controls. (**c**) Scatter plot representing mean fluorescence intensities of *P. aeruginosa* versus *S. aureus* cells attached to all topographies in the PS TopoChip.

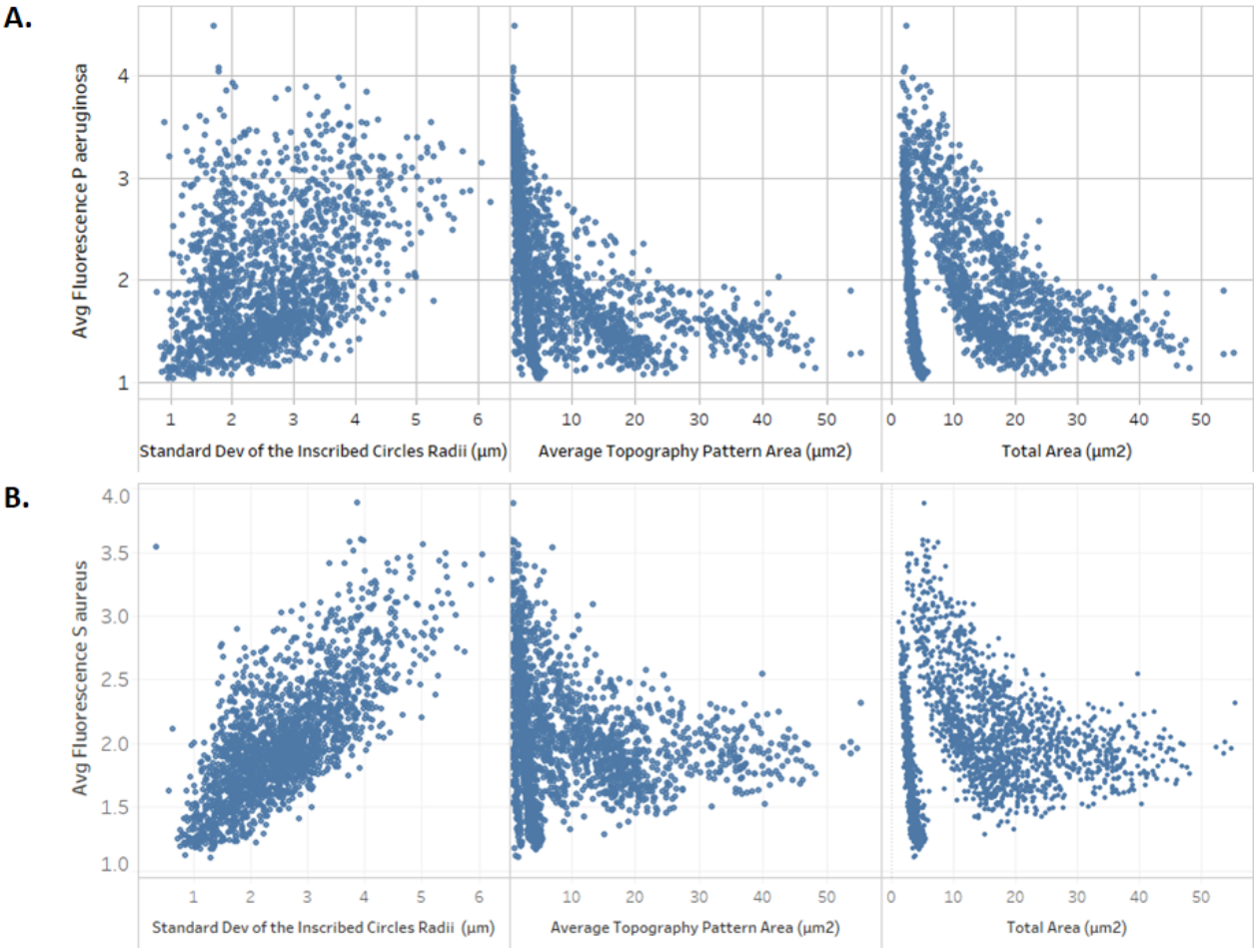

Figure S4. Topographical descriptors that show high correlation with bacterial attachment*:* (**a**) *P. aeruginosa* attachment; and (**b**) *S. aureus* attachment. The topographical descriptors found to be most important for bacterial attachment are the inscribed circles, which relate to the space between primitives, the average area covered by single primitives and the total area covered by primitives.

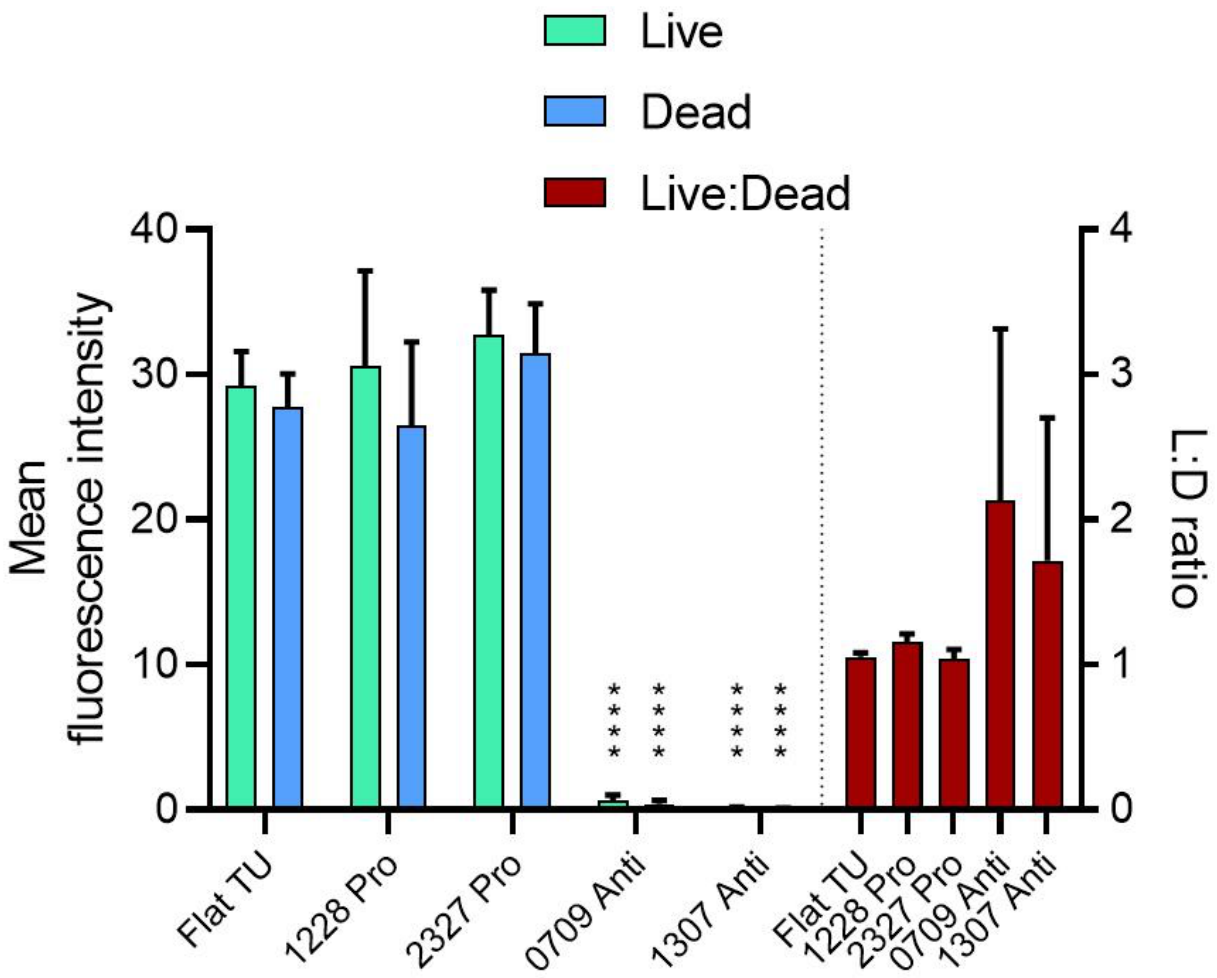

Figure S5. Mean fluorescence intensity of *P. aeruginosa* live/dead cells attached to flat, pro- (T2-PS-1228 and T2-PS-2327) and anti-attachment (T2-PS-0709 and T2-PS-1307) TUs after 4 h incubation in static conditions. The ratios of live/dead cells attached to each TU are also shown (right Y-axis). Data shown are mean ±SD, n = 7. Statistical analysis was done using a two-way ANOVA with Dunnett's multiple comparisons test (* $p<0.05$; ** $p<0.01$; *** $p<0.001$; **** $p<0.0001$).

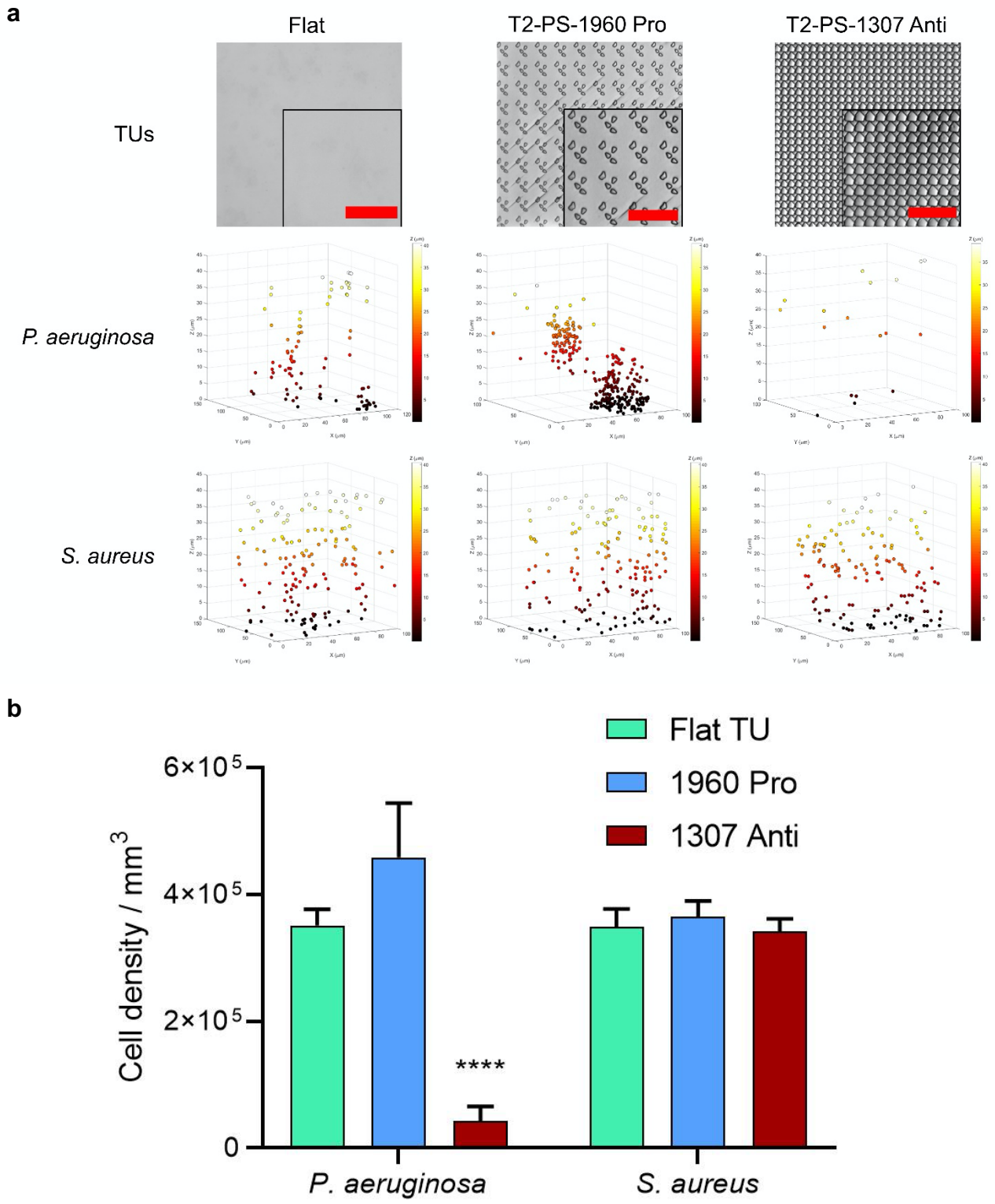

Figure S6. (**a**) *P. aeruginosa* and *S. aureus* cell population densities captured in the bulk medium immediately above the surface of flat, pro- (T2-PS-1960) and anti- attachment (T2-PS-1307) TUs after 3 hours exposure in static conditions. (**b**) The number of cells captured in 40 µm image stacks above the selected TU surfaces was quantified for both bacteria. Scale bar: 50 µm. Data shown are mean ±SD, n = 3. Statistical analysis was done using a two-way ANOVA with Dunnett's multiple comparisons test (* $p<0.05$; ** $p<0.01$; *** $p<0.001$; **** $p<0.0001$).

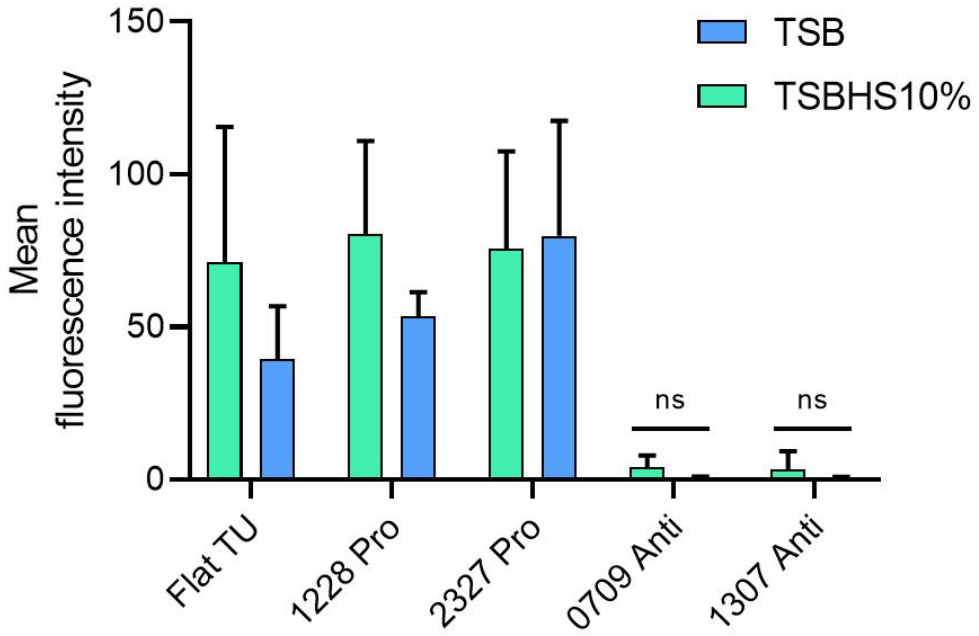

Figure S7. Comparative attachment of *P. aeruginosa* on flat, pro- (TS-PS-1228 and TS-PS-2327) and anti- attachment (TS-PS-0709 and TS-PS-1307) TUs in TSB or TSBHS10%. Data shown are mean ±SD, n ≥ 8. Statistical analysis was done using a two-way ANOVA with Dunnett's multiple comparisons test (ns $p>0.05$).

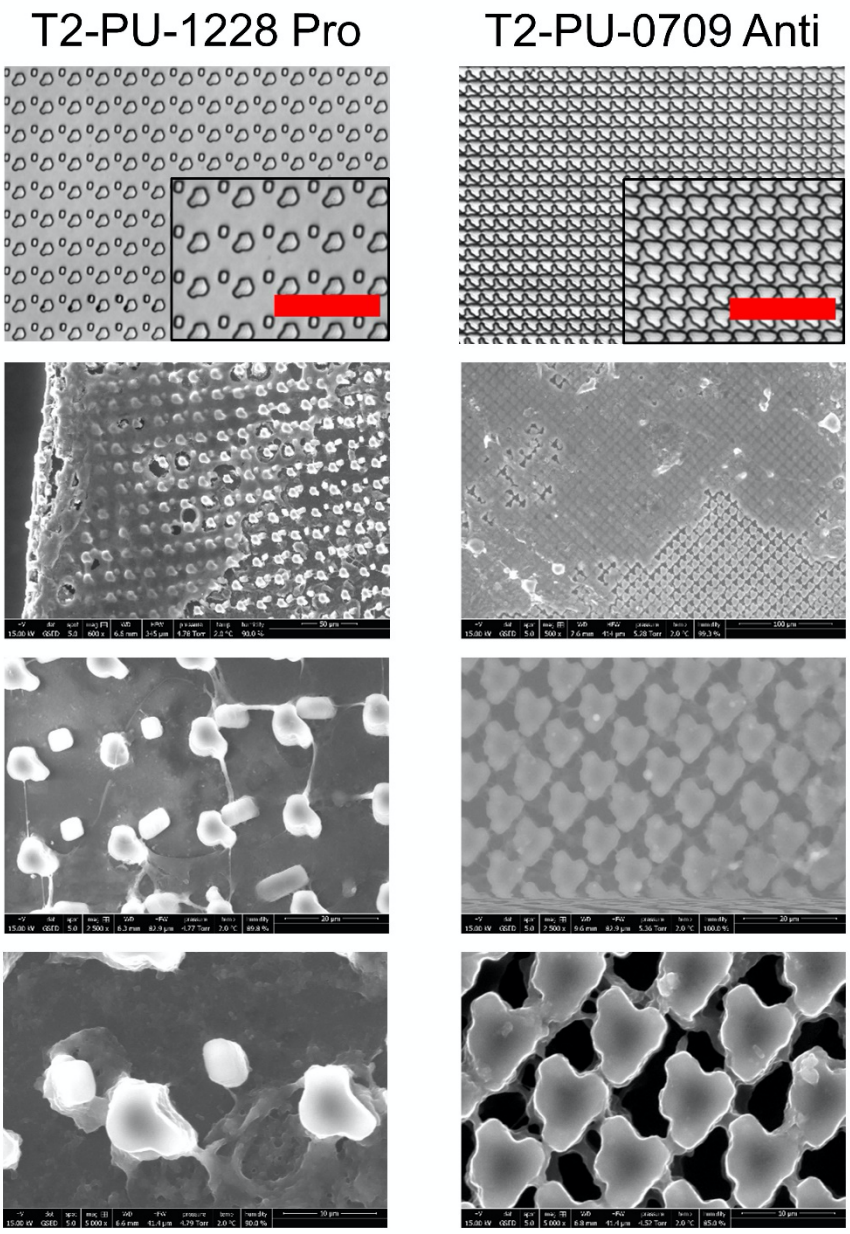

Figure S8. *Ex vivo* ESEM images of pro- (T2-PU-1228) and anti-attachment (T2-PU-0709) PU TUs removed from mice infected with *P. aeruginosa* for 4 days and imaged by ESEM. Scale bar in top row bright field images: 50 µm.

a Pro-attachment TopoUnit T2-PU-1228

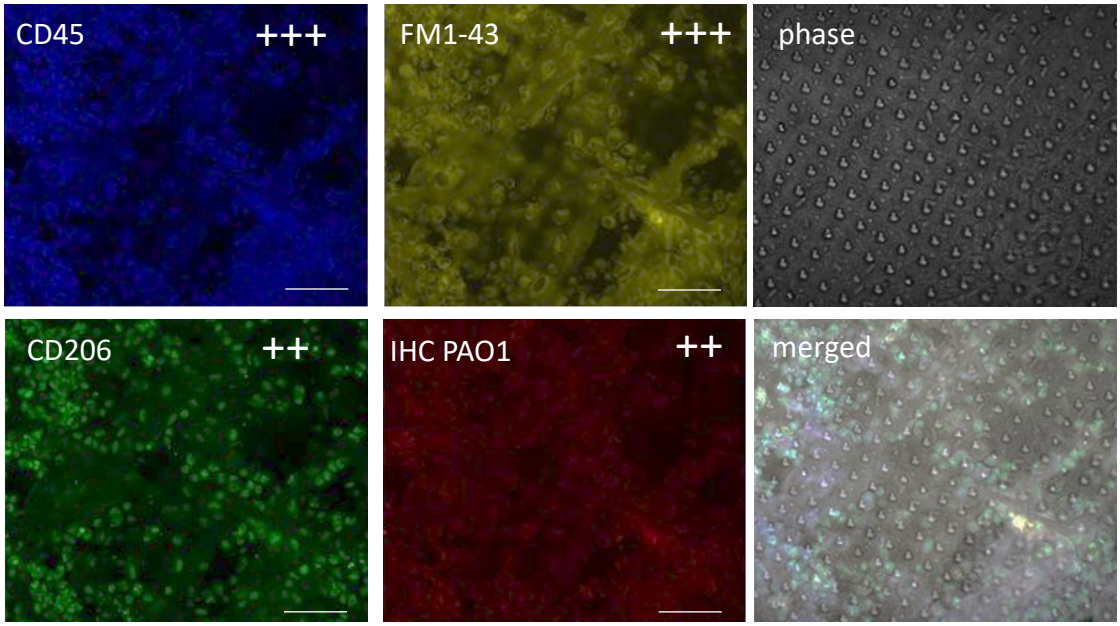

b Anti-attachment TopoUnit T2-PU-1307

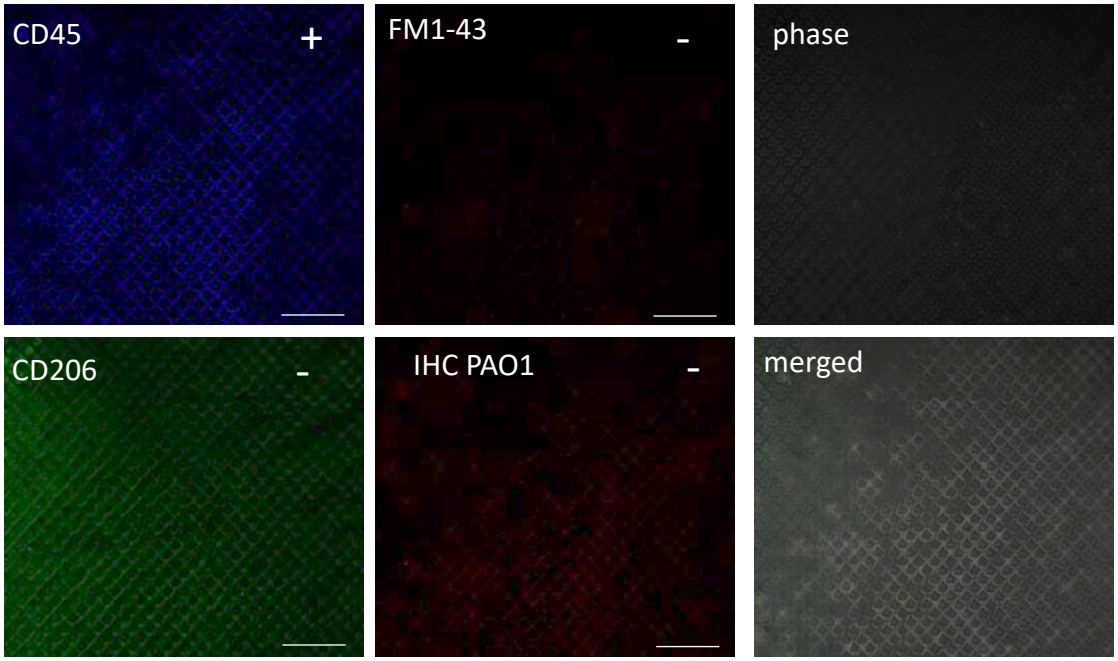

Fig. S9 Examples of confocal fluorescence, phase contrast and merged microscope images of the surfaces of a pro- (T2-PU-1228) (**a**) and an anti- (T2-PU-1307) (**b**) attachment PU Topo unit removed from the mice after 4 days post-infection and stained for *P. aeruginosa* (IHC), leucocytes (CD45) macrophages (CD206) or total cell biomass (FM1-43). For the semi-quantitative comparisons presented in **Table 1**, the bacterial and host cell populations interacting with each panel were scored -, not detected; +, low level; ++, intermediate; +++, high level. Examples of the scores are denoted on each of the four relevant 4 panels for the pro- and anti-attachment TUs in (**a**) and (**b**) above. Scale bar, 50 μM